Published in final edited form as:
Biochemistry. 2006 July 25; 45(29): 8894–8902. doi:10.1021/bi060534y.

Spectroscopic Analysis of Benzylidene Anabaseine Complexes with Acetylcholine Binding Proteins as Models for Ligand–Nicotinic Receptor Interactions†

Todd T. Talley[‡], **Samar Yalda**[‡], **Kwok-Yiu Ho**[‡], **Yitzhak Tor**[§], **Ferene S. Soti**[‖], **William R. Kem**[‖], and **Palmer Taylor**[‡,*]

[‡]Department of Pharmacology, University of California, San Diego, La Jolla, California 92093-0636

[§]Department of Chemistry-Biochemistry, University of California, San Diego, La Jolla, California 92093-0358

[‖]Department of Pharmacology and Therapeutics, University of Florida College of Medicine, Gainesville, Florida 32610-0267

Abstract

The discovery of the acetylcholine binding proteins (AChBPs) has provided critical soluble surrogates for examining structure and ligand interactions with nicotinic receptors and related pentameric ligand-gated ion channels. The multiple marine and freshwater sources of AChBP constitute a protein family with substantial sequence divergence and selectivity in ligand recognition for analyzing structure–activity relationships. The purification of AChBP in substantial quantities in the absence of a detergent enables one to conduct spectroscopic studies of the ligand–AChBP complexes. To this end, we have examined the interaction of a congeneric series of benzylidene-ring substituted anabaseines with AChBPs from *Lymnaea*, *Aplysia*, and *Bulinus* species and correlated their binding energetics with spectroscopic changes associated with ligand binding. The anabaseines display agonist activity on the α7 nicotinic receptor, a homomeric receptor with sequences similar to those of the AChBPs. Substituted anabaseines show absorbance and fluorescence properties sensitive to the protonation state, relative permittivity (dielectric constant), and the polarizability of the surrounding solvent or the proximal residues in the binding site. Absorbance difference spectra reveal that a single protonation state of the ligand binds to AChBP and that the bound ligand experiences a solvent environment with a high degree of polarizability. Changes in the fluorescence quantum yield of the bound ligand reflect the rigidification of the ring system of the bound ligand. Hence, the spectral properties of the bound ligand allow a description of the electronic character of the bound state of the ligand within its aromatic binding pocket and provide information complementary to that of crystal structures in defining the determinants of interaction.

Nicotinic acetylcholine receptors are prototypical members of the ligand-gated ion channel superfamily of receptors that include 5-HT_3, GABA-A and -C, and glycine receptors. Nicotinic receptors are found at the neuromuscular junction and throughout the nervous system, where they exist as either homomeric or heteromeric pentamers of subunits

†Supported by USPHS Fellowships NS 043063 to T.T.T., RO1-MH61412 to W.R.K., and R37-GM18360 to P.T.

*To whom correspondence should be addressed. Phone: 858-534-1366. Fax: 858-534-8248. pwtaylor@ucsd.edu.

†Supported by USPHS Fellowships NS 043063 to T.T.T., RO1-MH61412 to W.R.K., and R37-GM18360 to P.T.

encircling a central pore in a rosette arrangement. Contemporary understanding of the molecular structure of nicotinic receptors has benefited greatly from the discovery and subsequent X-ray crystal structures of a homologue of their extracellular ligand binding domain first identified in the freshwater snail, *Lymnaea stagnalis* (1, 2). Since this initial discovery, acetylcholine binding proteins (AChBPs1) have been identified in the molluskan species, *Bulinus truncatus*, and the marine-species, *Aplysia californica* (3, 4). The ensuing crystal structures of these nicotinic receptor surrogates have allowed an unprecedented atomic scale view of the binding site for the nicotinic ligands: nicotine (**1**), carbamylcholine, epibatidine (**2**), methyllycaconitine, and lobeline (5, 6) as well as peptide toxins from *Elapid* snakes and *Conus* snails (6–8).

The prevalence of nicotinic receptors in mediating physiological functions and the potential role of their altered function in disease states make them attractive targets for the development of new therapeutic agents. Despite the sequence and structural similarities between the AChBPs and nicotinic receptors, their ligand recognition characteristics have distinctive features. The availability of milligram quantities of expressed forms of the AChBPs as soluble proteins suitable for crystallography, spectroscopy, and high throughput drug screening make them uniquely suited for rigorous structure–activity studies.

To date, structure–activity analyses defining the determinants of selectivity for a series of congeneric ligands interacting with all three binding proteins have not been undertaken. Certain families of ligands should be particularly advantageous for such analyses because their physical properties may reveal differences in the protonation and electronic character of the free and bound states. For this reason, we have selected the substituted anabaseines (9, 10), a series of close congeners with spectroscopic properties that are sensitive to pH and their immediate solvent or binding site environment.

Anabaseine **3**, an alkaloid structurally related to nicotine (Figure 1, Table 1), was first identified in nemertine worms that use the compound for both defense and predation (11). It is a potent, though nonselective, mixed agonist/antagonist of neuronal nicotinic receptors (12). The benzylidene derivatives of anabaseine show greatly enhanced selectivity for α7 nicotinic receptors, presumably because of an increased interaction surface and enhanced conjugation in the core structure (9, 13). In addition, some benzylidene anabaseine (BA) compounds have been shown to have activity at 5-HT_{3A} receptors (14). The BA derivative 3-(2, 4-dimethoxybenzylidene)-anabaseine (**18**) (DMXBA or GTS-21) has been shown to be neuroprotective, cognition-enhancing and to alleviate deficits in auditory gating (10, 15, 16). This compound has also shown efficacy in smoking cessation and is currently in clinical trials for the treatment of schizophrenia (17, 18).

In the current study, we examine the binding affinities for a series of 24 structurally related anabaseine compounds for the three AChBPs of known crystal structures and compare binding energetics with those of the traditional ligands, nicotine and epibatidine. Using a combination of fluorescence and absorption spectroscopic measurements, we describe the electronic characteristics of the bound state of several anabaseine derivatives.

METHODS

Ligands and Reagents

Methyllycaconitine citrate was purchased from Tocris (Ellisville, MO). [^{3}H]-Epibatidine (specific activity: 55.5 Ci/mmol) was a product of Perkin-Elmer Life and Analytical

[1]Abbreviations: AChBP, acetylcholine binding protein; *Ls, Lymnaea stagnalis; Ac, Aplysia californica; Bt, Bulinus truncatus*; An, anabaseine; DMXBA, 3-(2, 4-dimethoxybenzylidene)-anabaseine; BA, 3-benzylidene anabaseine.

Sciences. Anabaseine compounds were synthesized as described previously (10). All other reagents were of the highest quality commercially available.

Expression and Purification of AChBPs

AChBPs from *Lymnaea stagnalis* (*Ls*), *Aplysia californica* (*Ac*), and *Bulinus truncatus* (*Bt*) were expressed using cDNAs synthesized from oligonucleotides engineered for mammalian codon usage, as previously described (4, 19, 20). Briefly, the AChBP gene was inserted into a FLAG-CMV-9 expression vector (Sigma) with the aminoglycoside phosphotransferase II gene, to confer aminoglycoside resistance, and a preprotrypsin leader peptide followed by a NH_2-terminal FLAG epitope. AChBP-transfected HEK-293 cells were selected with G418 to generate stably expressing cell lines. Dulbecco's modified Eagle's medium (MediaTech CellGro) containing 3% fetal bovine serum was collected at 3 day intervals from multitier flasks for up to 4 weeks. Adsorption onto anti-FLAG M2 affinity gel followed by elution with the FLAG peptide (both from Sigma) yielded purified protein in quantities between 0.5 and 5 mg/L of media. The purity and assembly of subunits as a pentamer were assessed by SDS–PAGE and fast protein liquid chromatography.

Two AChBP homologues (*Bt*-AChBP and *Bt*-AChBP-2) that differ by eight residues have been identified in the tissue of *Bulinus truncatus* (3). Our initial attempts expressing *Bt*-AChBP showed low expression in our system. During the process of converting *Bt*-AChBP to *Bt*-AChBP-2 by mutagenesis, we observed that the single mutation, F149L, results in the comparatively robust expression of a soluble pentameric entity. We used this construct for this investigation.

Radioligand Competition Assays

An adaptation of a scintillation proximity assay was used to determine the apparent K_d value as reported previously (20). Briefly, AChBP (final concentration ~500 pM binding sites), polyvinyltoluene anti-mouse SPA scintillation beads (0.1 mg/mL, Amersham Biosciences), monoclonal anti-FLAG M2 antibody from mouse (Sigma), and [^{3}H]-epibatidine (5 nM final concentration for *Ls* and *Bt*, 20 nM for *Ac*) were combined in a phosphate buffer (0.1 M, pH 7.0) with increasing concentrations of the competing ligand in a final volume of 100 μL. Total binding was determined in the absence of the competing ligand, and nonspecific binding was measured by adding a saturating concentration (15 μM) of methyllycaconitine. The resulting mixtures were allowed to equilibrate at room temperature for a minimum of 2 h and measured on an LS 6500 liquid scintillation counter (Beckman Scientific). The data obtained were normalized, fit to a sigmoidal dose–response curve (variable slope), and the K_d calculated from the observed EC_{50} value (21) using GraphPad Prism version 4.02 for Windows (San Diego, CA). A minimum of three independent experiments, performed in duplicate, were used to determine the K_d values reported. This procedure required less than 10 μg of each binding protein for this study, including initial compound screening and preliminary assays.

Spectrofluorometric Assays

Steady-state emission spectra were measured at room temperature, in a 0.1 M $NaPO_4$ binding buffer at pH 7.0, using a Jobin Yvon/Spex Fluoro-Max II spectrofluorometer (Instrument S. A., Inc., Edison, NJ) with the excitation and emission bandwidths set at 5 nm. Output is measured by photon counting and expressed in terms of counts per second (CPS). All fluorescence emission data are means of at least three replicate experiments with *Ls*-AChBP.

Absorption Spectra and Difference Spectra

The absorption spectra for substituted anabaseines in the various solvents, in a 0.1 M $NaPO_4$ binding buffer at pH 7.0, and in the pyrophosphate–phosphate mixture to vary pH were measured in a double beam Cary 15 spectrophotometer. Difference spectra were measured using matched tandem mixing cells in each beam, where AChBP in slight stoichiometric excess of binding sites and substituted BA in a 0.1 M $NaPO_4$ buffer were placed in separate 0.42 cm compartments in both the sample and reference cuvettes. A spectrum was then run to ensure concentration balance. The solutions were mixed in the sample beam cuvette and the difference spectra collected. Following the mixing of solutions in the reference beam, the spectrum was again recorded to ensure balance of concentrations after mixing both cuvettes.

The difference spectra for the bound ligand at two pH values, chosen to distinguish between the ionization states of the free ligand, were run in standard 1 cm cuvettes in 0.1 M $NaPO_4$. Requisite amounts of concentrated Na_2HPO_4 or NaH_2PO_4 were added to adjust the pH to the specified pH value.

RESULTS

Comparison of Anabaseine Binding Affinities for the Three AChBPs

The recently deposited crystal structures of the three AChBPs with a variety of ligands (3, 5–8) and an apostructure (6) provide a comprehensive view of the primary ligand binding domain and a structural template for nicotinic receptors and other members of the LGIC family of receptors. When comparing ligand affinities obtained from the three AChBP species (Figure 1), several observations are noteworthy. In general, the rank ordering of affinities for this series of compounds show reasonable correlations between the three species. Sub-nanomolar K_d values were found for several compounds, but the parent anabaseine itself had a K_d of ~200 nM. It ranked among the least potent member of the set. AChBP's from *Ls* and *Ac* show the greatest sensitivity to structure variations in the family of substituted anabaseine compounds. The range of K_d denotes a selectivity of roughly 3000-fold between the strongest and weakest of the ligands for *Ac*-AChBP compared to the nearly 500-fold difference observed for *Ls*-AChBP and the 150-fold difference for *Bt*-AChBP (Figure 2). Anabaseine (An) was one of the weakest ligands for *Ac*-AChBP but had moderate affinity for the AChBP from *Bt*.

The anabaseine analogue, PTHP **4** (see chemical name in footnote a, Table 1), exhibited very low affinities for all three species. That rearrangements of the pyridine nitrogen position in the An moiety are poorly tolerated is also evident for the comparatively low affinities of DMXB–IsoA **6** with the AChBP from the three species (Table 1). The removal of the conjugation between the pyridine and imine nitrogens (DMXBzAi, **5**) also decreased affinity. The addition of the benzylidene functionality to generate 3-benzylidene anabaseine (BA, **7**), resulted in a 7-fold increase in affinity for *Bt*-AChBP, whereas the benzylidene moiety increased in affinity for the *Ls*- and *Ac*-AChBPs 17- and 890- fold, respectively. This increase in affinity differs from the observed decrease in affinity for the mammalian α7 and α4β2 receptors with the addition of the benzylidene ring (10, 12).

The four compounds with the highest affinity for both the *Ls*- and *Ac*-AChBPs had either a hydroxyl or an amino substitution in the 4- position of the benzylidene ring. The addition of a hydroxyl to the 4-position of BA to generate **12** increases affinity 25-fold for *Ls*-AChBP, whereas the influence of this substitution is more modest for the *Ac*- and *Bt*-AChBPs, increasing affinity only 2- and 5-fold, respectively. The influence of benzylidene substitution is dependent upon both the position and nature of the substituents. A negligible change in affinity (less than 2-fold) follows the addition of a hydroxyl to the 3- position of BA for both the *Ls* and *Ac* constructs, whereas this substitution is poorly tolerated by *Bt*,

resulting in a 20-fold reduction in affinity. In contrast, 2-OHBA **8** is only slightly less potent than the unsubstituted BA for both *Ls* and *Bt* but is 10-fold less potent for *Ac*. Simple substitution at the 4-position does not necessarily ensure greater affinity as demonstrated by the negligible change observed between BA and 4-MeOBA **13** for the *Ls*- and *Bt*-AChBP and the 10-fold decrease for the *Ac*-AChBP. This trend is reinforced by the low relative affinities of the electron-withdrawing 4-cyano benzylidene (**17**) for all of the AChBPs.

The addition of a methoxy group (OCH_3) to both the 2- and 4-positions of the BA structure to generate DMXBA has little effect on affinity for the *Ls*-AChBP, whereas decreasing the affinity 36-fold for the *Ac*-AChBP and increasing the affinity slightly for the *Bt*-AChBP. The addition of a third methoxy group to the 6-position to form TMXBA **25** is poorly tolerated in all cases. In contrast, the 4-OH metabolite of DMXBA, 2-MeO 4-OHBA **21**, is the most potent compound of the set for all three species. The conversion of DMXBA to its 2-OH derivative, 2-OH 4-MeOBA **19**, has relatively little effect on the observed affinity for all three AChBPs, whereas the dihydroxy derivative 2, 4-DiOHBA **22** shows a 25- and 55-fold increase in affinity relative to that of DMXBA for *Ls*- and *Ac*-AChBPs, respectively, but a more than 2-fold decrease for *Bt*.

Influence of pH on Ligand Binding

To explore further the role of the ionization state on the binding energetics, a series of radioligand binding assays were conducted by competition with [^{3}H]-epibatidine on a subset of four compounds at pH values over the 6 to 9 range (Figure 3). The observed IC_{50} values for BA, DMXBA, and the hydroxyl metabolites of DMXBA decreased at lower pH values suggesting that the protonated form of these ligands has a greater affinity for the binding proteins than the nonionized form. The binding profile of [^{3}H]-epibatidine with its pK_a of 10.1 was relatively unchanged over this pH range. Accordingly, the observed differences in binding affinities with pH are likely due to ionization equilibria on the anabaseine congeners rather than on the ionizable side chains in the binding protein. The shift of the curves to lower concentration as the pH decreases is consistent with the bound species being protonated on the imine nitrogen. Similar results were found for DMXBA binding to rat α7 receptors (10).

Spectroscopic Analysis of the Anabaseine Derivatives at Various pH Values

To describe the molecular environment and ionization state of the bound ligands relative to their free state, absorbance and fluorescence spectra were collected initially for each compound in the reference buffer. Then subsets of substituted anabaseines with sufficient affinity and interesting spectral characteristics were subjected to an examination of the influence of pH and solvent environment on their spectra.

For most of the compounds, a comparison of absorbance measured in a phosphate/pyrophosphate buffer from pH 5.0 to 9.0 in 0.5 pH unit increments shows the presence of a virtual isosbestic point indicative of two primary chromophoric ionization states (Figure 4A). This allowed for an estimate of the apparent pK_a value for the tetrahydropyridine nitrogen (Table 2) with results in reasonable agreement with previously reported values (10).

The spectra for all of the benzylidene anabaseines except for those with a phenolic group on the benzylidene ring exhibit an increase in absorbance of the long wavelength peak with a decrease in pH. Hence, the protonation of the imine nitrogen in the tetrahydropyridine ring results in the lower energy chromophore primarily encompassing benzylidene to the tetrahydropyridine conjugated system. Uniquely, within the series, the 2- and 4-hydroxyl substituted BA compounds not only show an emergence of a long wavelength peak but also the increase in the intensity of this peak with pH (Figure 4B). Extending the titration from

pH 9.0 to 11 resulted in no further wavelength shift in absorption maxima but slight differences in intensity (data not shown). The stabilization of a zwitterionic species with protonated imine nitrogen and the phenolate anion serves to lower the pK_a for formation of the zwitterion. Hence, this ionization state likely predominates at physiological pH. The isosbestic point with the phenolic congeners is not as well defined, suggesting the presence of small amounts of singly ionized species. Titration curves are shown for two representative benzylidenes (Figure 4A and B). The pK_a values determined from these curves and other spectroscopic characteristics of the anabaseine derivatives are listed in Table 2.

Absorption Spectra for Bound Anabaseine Derivatives

When DMXBA and 2-MeO 4-OHBA are bound to AChBP, a bathochromic shift to longer wavelength is seen (Figure 4C and D). The measurements of difference spectra for DMXBA bound to AChBP at two pH values, 7.1 and 8.1, that span the solution pK_a determined spectroscopically show only small excursions from the zero line, establishing that the protonated imine species is the bound entity (Figure 4E). Similarly, only a small difference spectrum is generated for 2-MeO 4-OHBA between pH 6.6 and 7.6, indicating that the bound ligand species does not lose a proton over this pH range (Figure 4F). The concentration of the binding protein exceeds the K_d value at pH 7.0 by 3 orders of magnitude. Consequently, over this range of pH values, at least 99% of the ligand should be bound. Hence, neither the phenolic hydrogen nor the protonated imine are titratable in the bound state.

Anabaseine Difference Spectra

Where permitted by solubility, we also examined the wavelength dependence in solvents of varying polarizability and relative permittivity (formerly called the dielectric constant) (Figure 5). In general, the solvents of increasing polarizability and decreasing relative permittivity shift the substituted anabaseine wavelength maximum to the longer wavelength. Moreover, a marked substituent effect on the wavelength maxima can be demonstrated to correlate with the Hammett substituent coefficient (Figure 6) (22). The difference spectra of the binding protein–ligand complex measured in the mixed versus unmixed tandem cell show the presence of only the ionized form of the imine for each compound (Figure 5). The bathochromic shift or positive solventochromic shift (23) is characteristic of the apolar environment shown with the solvents (Table 3).

A clear spectral distinction is seen in pH dependence of the spectra, where the peak heights of the long and short wavelength peaks show a reciprocal relationship but no shift in wavelength. In contrast, the wavelength maximum of the predominant peak is dependent on the relative permittivity and polarizability of the medium (23).

Fluorescence Spectra of the Anabaseine Derivatives

The set of substituted anabaseines, despite their extended conjugation, show low fluorescence quantum yields in an aqueous buffer (Figure 7). As expected from their spectral overlap with tryptophan emission, all of the substituted benzylidene anabaseines quenched the intrinsic fluorescence of the AChBPs when bound (data not shown). However, several of the substituted anabaseines, the *p*-amino **15**- and *p*-dimethylamino **16**-substituted derivatives in particular, exhibit large (~100-fold) enhancements of fluorescence when bound (Figure 7A). The fluorescence enhancement in the bound state likely reflects the constraints on the torsional bond motion of the excited state of the chromophore (24).

The large enhancement of the fluorescence quantum yield of the amino-substituted BAs, coupled with their high affinities for the binding proteins, confer valuable properties to this

subfamily of substituted anabaseines for ascertaining the stoichiometry of binding and for estimating the dissociation constants for nonfluorescent ligands by competition. Shown in Figure 7C are the titrations conducted at ligand and AChBP concentrations that exceed the K_d, thereby revealing a stoichiometry of ligand binding approximating one ligand per subunit. Competition is shown with epibatidine (Figure 7D), revealing the mutually exclusive binding of the two ligands and a common stoichiometry with epibatidine. Previous studies have shown a 1:1 complex with each AChBP subunit for epibatidine (19).

DISCUSSION

AChBPs from three invertebrate species show considerable divergence in sequence and, thus, provide soluble proteins with distinctive specificities for agonists and antagonists that associate with the various nAChR subtypes. Previous studies have not only shown a nicotinic ligand specificity for the binding proteins but also the kinetic characteristics typical of ligand recognition for nicotinic receptors (1–3, 5–7). For example, the three-fingered toxins show slow rates of association and dissociation with the binding protein, whereas the association of agonists, such as acetylcholine, is rapid, approaching the diffusion limit (19). Certain alkaloids and peptide toxins show a high degree of selectivity of binding for AChBPs from different species. For example, α-conotoxin ImI and lobeline show ~10 000- and 300-fold greater affinities for the *Aplysia* binding protein than that for *Lymnaea*, whereas the α-neurotoxins show a 100-fold preference for *Lymnaea* (4).

By the expression of a cDNA chimera of AChBP and the receptor, the *Lymnaea* protein has been linked to the *C*-terminal transmembrane-spanning region of a ligand-gated ion channel. The expressed protein assembles as a pentamer and, when expressed with transmembrane spans, shows agonist-elicited channel opening characteristics of the nicotinic receptor (25). Thus, the AChBPs present a family of proteins that can be expressed in substantial quantities and are sufficiently robust so that nicotinic receptor selectivity can be maintained in the face of substantial changes in the sequence. Accordingly, through mutagenesis, it should be possible to replicate the binding surfaces of the naturally occurring nicotinic receptor subtypes and other members of the Cys-loop receptor family.

Anabaseine Alkaloids

The large number of benzylidene-substituted anabaseine analogues that have been synthesized (13, 26) make them an ideally suited series of congeners for a detailed analysis with the ligand binding sites on the three AChBPs examined here. Interestingly, the core anabaseine structure has a lower affinity for the AChBPs (K_d = 240, > 1000, and 830 nM) than for the α7 (rat) receptor (K_d = 58 nM) (12). However, upon benzylidene substitution, high affinities reappear, and in fact, some of the analogues in Table 1 show far higher affinities for AChBPs than the α7 receptor (13), with K_d values in the subnanomolar range. Structural modifications leading to a loss of conjugation and repositioning of the imine or pyridine nitrogens result in diminished affinity for all three binding proteins.

A general correlation in binding energies is seen for benzylidene anabaseine interactions with the three AChBPs (Figure 2). The greatest range of affinities in the low concentration range comes from *Aplysia*. Some of the outlying members of these correlational plots should be of interest for delineating the determinants giving rise to the affinity differences. In general, electron-withdrawing groups on the benzylidene ring decrease AChBP affinity, whereas electron donors show an enhancement of affinity. Electron-donating effects also increase the basicity of the imine nitrogen, facilitating the retention of the proton over a physiologic pH range.

Substituted benzylidene analogues of anabaseine give rise to sufficient conjugation in the molecule so that their long wave absorption bands fall outside of the range of the protein envelope and are sensitive to characteristics of the solvent environment and the protonation state of the imine nitrogen. Moreover, the amino benzylidene-substituted anabaseines also are fluorescent and show large enhancements in quantum yield upon binding to the protein.

The unique conjugation profiles and ionization states of the BA congeners provide information that should be complementary to the crystallographic studies of the complex with AChBP. In the core anabaseine molecule, a pyridine linked to a nitrogen-containing aliphatic ring is also characteristic of nicotine and its analogues. Therefore, this portion of the anabaseine molecule may bind in a similar orientation, which would place the imine nitrogen near tryptophan 147 in *Ac*-AChBP, near the subunit interface. On the basis of the nicotine and epibatidine complexes (3, 5, 6), the protonated amine would be expected to interact with the carbonyl group of tryptophan 147 and to be lodged near the electron rich aromatic residues in the binding pocket. In addition to the interaction with the Trp 147 carbonyl, the protonated imine with its extended conjugation would interact with the electron-rich tyrosine and tryptophan side chains in the binding pocket (Trp 147, Tyr 93, Tyr 188, Tyr 195) (Figure 8). Such a nest of tethered aromatic side chains not only provides an immediate hydrophobic environment but also one with a high degree of polarizability.

Visible Difference Spectroscopy and Fluorescence Spectroscopy

A comparison of the spectra of the bound BA relative to that of the free species in various solvents and buffers has enabled us to describe the ionization state and proximal environment conferred by the determinants of anabaseine binding at the subunit interface. With the BA compounds studied, over a physiologic pH range, only the imine nitrogen has the potential of protonation. When the BA compounds are protonated, a bathochromic shift is evident with the long wavelength peak appearing at 398 nm. A fairly well-defined isosbestic point in the titration of the nonhydroxyl-substituted BA clearly reflects the primary involvement of two chromophoric species. A difference spectrum for the free and bound **18** and **21** shows the imine protonated species to be bound (Figure 5E and F), a finding also consistent with the pH dependence of anabaseine binding. Similarly, an analysis of **18** and **21** binding at two pH values spanning their pK_a in solution also shows the protonated species as the bound entity (Figure 4E and F). Hence, the ionization state can be analyzed through the ratio of the long wavelength to short wavelength peaks.

The relative permittivity and polarizability of the surrounding media also influences the spectra (Figures 5 and 6). Here, the differences in solvent parameters affect the wavelength maxima of the peaks by virtue of stabilizing the ground state of the molecules (23). In this case, we note a bathochromic or positive solventochromatic shift with the increasing hydrophobicity of the solvent (Figure 5A) and with the binding of DMXBA (Figure 5C and E).

More complex pH dependent behavior is seen for the hydroxyl-substituted BA compounds with two titratable hydrogens and where multiple resonance species stabilize the phenolate anion. In addition, conferral of the positive charge on the imine nitrogen will also exert an inductive effect that should stabilize the zwitterion as in Scheme 1.

The deviations from the isosbestic point seen in the titration curves (Figure 4B), suggest the presence of a singly ionized species in low abundance. The pH difference spectra for the 2-MeO 4-OHBA, when bound to AChBP, show only a small excursion over the sensitive range for the titration of the free species (Figure 4F). Accordingly, the species with the protonated imine and phenol also appear to be the predominant bound species. The 4-

hydroxy BA compounds are among the highest affinity ligands in the series, and hydrogen bonding through the phenolic hydroxyl is likely to be contributory to the binding energetics.

A comparison of the shift in wavelength maxima, a property of the ground-state energy of the compounds, also reveals information on the electronic character of the bound state. Within the binding site, the crystal structures reveal an aromatic cluster of side chains with Trp and Tyr side chains outlining the binding site (1, 3, 6–8). Although the environment of extended aromatic residues cannot be replicated by a solvent or solvent mixture, the marked bathochromic shift in the wavelength maximum reflects the differences in the relative permittivity and polarizability of the subunit interface environment of the AChBP molecule.

The unique fluorescence characteristics of the amino-substituted BA in the bound state (Figure 7) reflect the behavior of the first excited state of these compounds (24). The alignment of the ring systems in the bound state enhances the depopulation from the excited state by light emission rather than the release of thermal energy. When the excitation spectra of the free and bound ligands are compared, the same bathochromic shift associated with ligand binding is evident in the fluorescence and absorption spectra (Figures 4 and 7).

Because of their unique spectroscopic properties, BA compounds enable one to detail the ionization state and electronic properties of the bound ligand through the use of difference absorption spectra and fluorescence properties of the bound molecule. The AChBPs facilitate such studies because in contrast to the nicotinic receptor, the proteins can be generated as homogeneous entities in mg quantities and in the absence of light scattering detergent micelles. The robust characteristics of AChBPs also present the prospect of modifying the binding interfaces to more closely resemble the individual receptor subtypes. Complementing the spectroscopic approach with crystallographic and mutagenesis studies of the complex should enable one to ascertain the interacting atomic determinants in great detail.

REFERENCES

1. Brejc K, van Dijk WJ, Klaassen RV, Schuurmans M, van Der Oost J, Smit AB, Sixma TK. Crystal structure of an ACh-binding protein reveals the ligand-binding domain of nicotinic receptors. Nature. 2001; 411:269–276. [PubMed: 11357122]
2. Smit AB, Syed NI, Schaap D, van Minnen J, Klumperman J, Kits KS, Lodder H, van der Schors RC, van Elk R, Sorgedrager B, Brejc K, Sixma TK, Geraerts WP. A glia-derived acetylcholine-binding protein that modulates synaptic transmission. Nature. 2001; 411:261–268. [PubMed: 11357121]
3. Celie PH, Klaassen RV, van Rossum-Fikkert SE, van Elk R, van Nierop P, Smit AB, Sixma TK. Crystal structure of acetylcholine-binding protein from Bulinus truncatus reveals the conserved structural scaffold and sites of variation in nicotinic acetylcholine receptors. J. Biol. Chem. 2005; 280:26457–26466. [PubMed: 15899893]
4. Hansen SB, Talley TT, Radic Z, Taylor P. Structural and ligand recognition characteristics of an acetylcholine-binding protein from Aplysia californica. J. Biol. Chem. 2004; 279:24197–24202. [PubMed: 15069068]
5. Celie PH, van Rossum-Fikkert SE, van Dijk WJ, Brejc K, Smit AB, Sixma TK. Nicotine and carbamylcholine binding to nicotinic acetylcholine receptors as studied in AChBP crystal structures. Neuron. 2004; 41:907–914. [PubMed: 15046723]
6. Hansen SB, Sulzenbacher G, Huxford T, Marchot P, Taylor P, Bourne Y. Structures of Aplysia AChBP complexes with nicotinic agonists and antagonists reveal distinctive binding interfaces and conformations. EMBO J. 2005; 24:3635–3646. [PubMed: 16193063]
7. Celie PH, Kasheverov IE, Mordvintsev DY, Hogg RC, van Nierop P, van Elk R, van Rossum-Fikkert SE, Zhmak MN, Bertrand D, Tsetlin V, Sixma TK, Smit AB. Crystal structure of nicotinic

acetylcholine receptor homolog AChBP in complex with an alpha-conotoxin PnIA variant. Nat. Struct. Mol. Biol. 2005; 12:582–588. [PubMed: 15951818]

8. Bourne Y, Talley TT, Hansen SB, Taylor P, Marchot P. Crystal structure of a Cbtx-AChBP complex reveals essential interactions between snake alpha-neurotoxins and nicotinic receptors. EMBO J. 2005; 24:1512–1522. [PubMed: 15791209]
9. Papke RL, Meyer EM, Lavieri S, Bollampally SR, Papke TA, Horenstein NA, Itoh Y, Porter Papke JK. Effects at a distance in alpha 7 nAChR selective agonists: benzylidene substitutions that regulate potency and efficacy. Neuropharmacology. 2004; 46:1023–1038. [PubMed: 15081799]
10. Kem WR, Mahnir VM, Prokai L, Papke RL, Cao X, LeFrancois S, Wildeboer K, Prokai-Tatrai K, Porter-Papke J, Soti F. Hydroxy metabolites of the Alzheimer's drug candidate 3-[(2,4-dimethoxy)benzylidene]-anabaseine dihydrochloride (GTS-21): their molecular properties, interactions with brain nicotinic receptors, and brain penetration. Mol. Pharmacol. 2004; 65:56–67. [PubMed: 14722237]
11. Kem WR. A study of the occurrence of anabaseine in Paranemertes and other nemertines. Toxicon. 1971; 9:23–32. [PubMed: 5539373]
12. Kem WR, Mahnir VM, Papke RL, Lingle CJ. Anabaseine is a potent agonist on muscle and neuronal alphabungarotoxin-sensitive nicotinic receptors. J. Pharmacol. Exp. Ther. 1997; 283:979–992. [PubMed: 9399967]
13. Stokes C, Papke JK, Horenstein NA, Kem WR, McCormack TJ, Papke RL. The structural basis for GTS-21 selectivity between human and rat nicotinic alpha7 receptors. Mol. Pharmacol. 2004; 66:14–24. [PubMed: 15213292]
14. Machu TK, Hamilton ME, Frye TF, Shanklin CL, Harris MC, Sun H, Tenner TE Jr, Soti FS, Kem WR. Benzylidene analogs of anabaseine display partial agonist and antagonist properties at the mouse 5-hydroxytryptamine(3A) receptor. J. Pharmacol. Exp. Ther. 2001; 299:1112–11129. [PubMed: 11714901]
15. Stevens KE, Kem WR, Mahnir VM, Freedman R. Selective alpha7-nicotinic agonists normalize inhibition of auditory response in DBA mice. Psychopharmacology (Berlin). 1998; 136:320–327. [PubMed: 9600576]
16. O'Neill HC, Rieger K, Kem WR, Stevens KE. DMXB, an alpha7 nicotinic agonist, normalizes auditory gating in isolation-reared rats. Psychopharmacology (Berlin). 2003; 169:332–339. [PubMed: 12759805]
17. Kitagawa H, Takenouchi T, Azuma R, Wesnes KA, Kramer WG, Clody DE, Burnett AL. Safety, pharmacokinetics, and effects on cognitive function of multiple doses of GTS-21 in healthy, male volunteers. Neuropsychopharmacology. 2003; 28:542–551. [PubMed: 12629535]
18. Olincy A, Harris JG, Johnson LL, Pender V, Kongs S, Allensworth D, Ellis J, Zerbe GO, Leonard S, Stevens KE, Stevens JO, Martin LF, Adler LE, Soti F, Kem WR, Freedman R. Proof-of-concept trial of an α7 nicotinic agonist in schizophrenia. Arch. Gen. Psychiatry. 2006; 63:630–638. [PubMed: 16754836]
19. Hansen SB, Radic Z, Talley TT, Molles BE, Deerinck T, Tsigelny I, Taylor P. Tryptophan fluorescence reveals conformational changes in the acetylcholine binding protein. J. Biol. Chem. 2002; 277:41299–41302. [PubMed: 12235129]
20. Hibbs RE, Talley TT, Taylor P. Acrylodan-conjugated cysteine side chains reveal conformational state and ligand site locations of the acetylcholine-binding protein. J. Biol. Chem. 2004; 279:28483–28491. [PubMed: 15117947]
21. Cheng Y, Prusoff WH. Relationship between the inhibition constant (K1) and the concentration of inhibitor which causes 50% inhibition (I50) of an enzymatic reaction. Biochem. Pharmacol. 1973; 22:3099–3108. [PubMed: 4202581]
22. Hansch C, Leo A, Taft RW. A survey of Hammett substituent constants and resonance and field parameters. Chem. ReV. 1991; 91:165–195.
23. Reichard C. Solvatochromic dyes as solvent polarity indicators. Chem. ReV. 1994; 94:2319–2358.
24. Lakowicz, JR. Principles of Fluorescence Spectroscopy. 2nd ed. New York: Kluwer Academic Publishers and Plenum Publishing Corp; 1999.

25. Bouzat C, Gumilar F, Spitzmaul G, Wang HL, Rayes D, Hansen SB, Taylor P, Sine SM. Coupling of agonist binding to channel gating in an ACh-binding protein linked to an ion channel. Nature. 2004; 430:896–900. [PubMed: 15318223]

26. Le Francois, SE.; Prokai, L.; Soti, F.; Kem, WR. 2004 Abstract Viewer/Itinerary Planner. Washington, D.C.: Society for Neuroscience; 2004. 2004

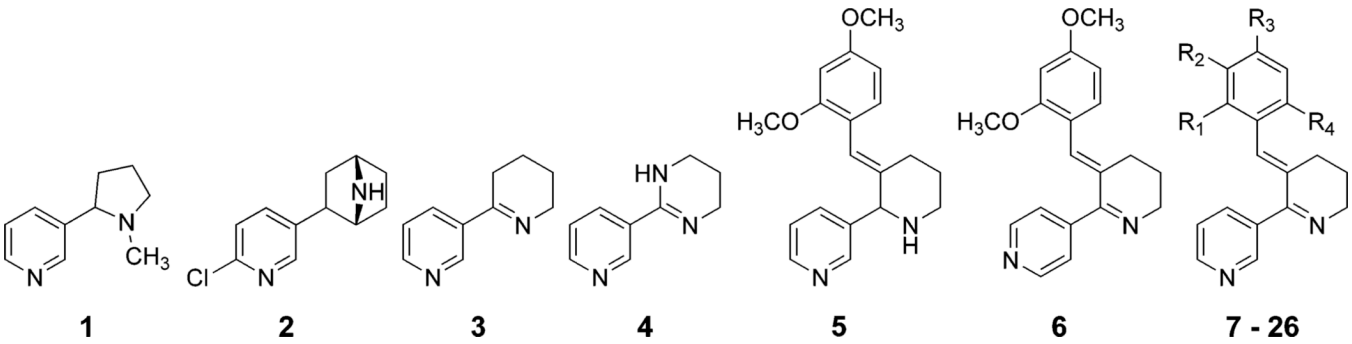

Figure 1.

Structures of nicotine **1**, epibatidine **2**, anabaseine **3**, 2-(3-pyridyl)-3,4,5,6-tetrahydropyrimidine (PTHP) (**4**), 3-(2,4-dimethoxybenzyl)-(±) anabaseine (DMXBzAi) (**5**), 2-(4-pyridyl)-3-(2,4-dimethoxybenzylidene)-4,5,6,-tetrahydropyridine (DMXB IsoA) (**6**), and benzylidene anabaseines **7–26**.

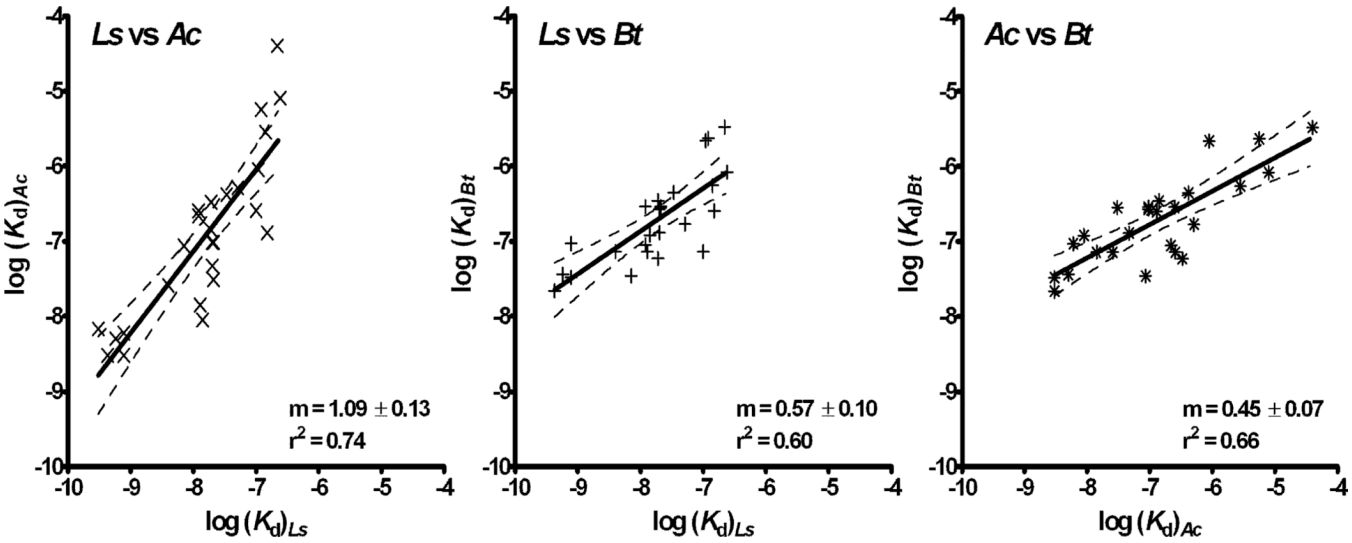

Figure 2.

Relationship between the dissociation constants, K_d, for ligand binding to the three acetylcholine binding proteins from *Lymnaea stagnalis* (*Ls*), *Aplysia californica* (*Ac*), and *Bulinus truncatus* (*Bt*). Data from Table 1 are plotted logarithmically to reflect the proportionate relationship of the free energies of binding, $\log(K) = -\Delta G/(2.3RT)$, for the various ligands.

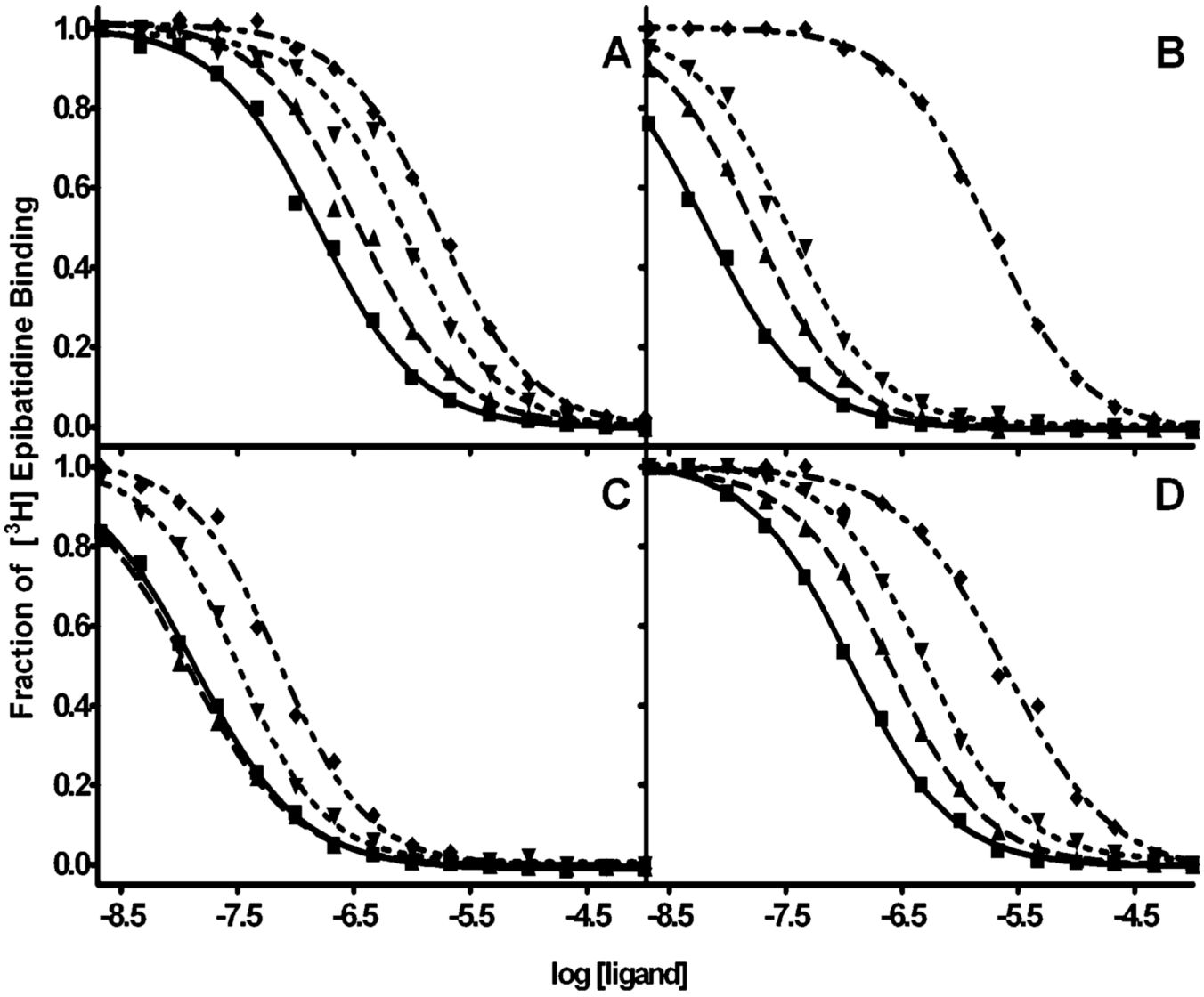

Figure 3.

Competition between the binding of the benzylidene anabaseine derivatives and [^{3}H]-epibatidine (pK_a = 10.1) to *Lymnaea* AChBP at various pH values. (A) DMXBA **18**; (B) 2-MeO, 4-OHBA **21**; (C) 4-NH_2BA **15**; (D) BA **7**. The pH of the 0.1 M phosphate/pyrophosphate buffer used: (■) pH 6, (▲) pH 7, (▼) pH 8, (♦) pH 9. The structures are shown in Figure 1.

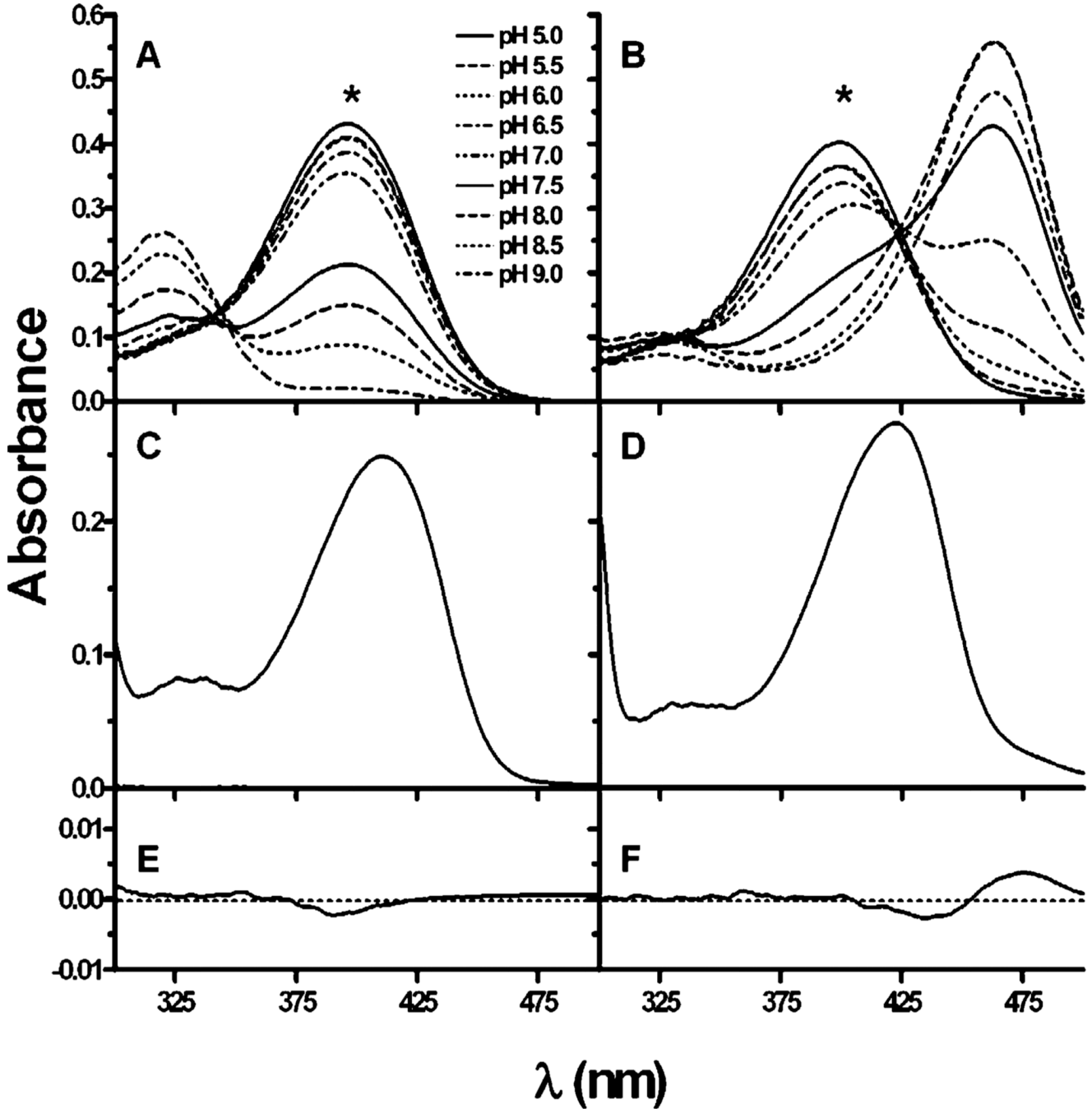

Figure 4.

Absorption spectra of 3-(2,4-dimethoxybenzylidene)-anabaseine (DMXBA, **18**) (A, C, E) and 3-(2-methoxy-4-hydroxybenzylidene)-anabaseine (2-MeO, 4-OHBA, **21**) (B, D, F) as a function of pH. (A) and (B) Representative absorption spectra as a function of pH (0.5 increments from pH 5.0 to 9.0) for DMXBA and 2-MeO, 4-OHBA. Note the position of the wavelength peaks and that the long wavelength peak decreases in intensity with increasing pH for DMXBA, whereas it increases for 2-MeO, 4-OHBA. (C) and (D) DMXBA and 2-MeO, 4-OHBA, respectively, bound to *Ls*-AChBP in pH 8.1 and a 7.6 M $NaPO_4$ buffer. (E) and (F) Difference spectra recorded for the complexes of the ligands with stoichiometric amounts of AChBP (30 μM of binding sites and 20 μM ligand). The spectra taken at pH

values of 0.5 pH units above and below the apparent pK_a value of each compound overlay closely, indicating the presence of a single ionization state.

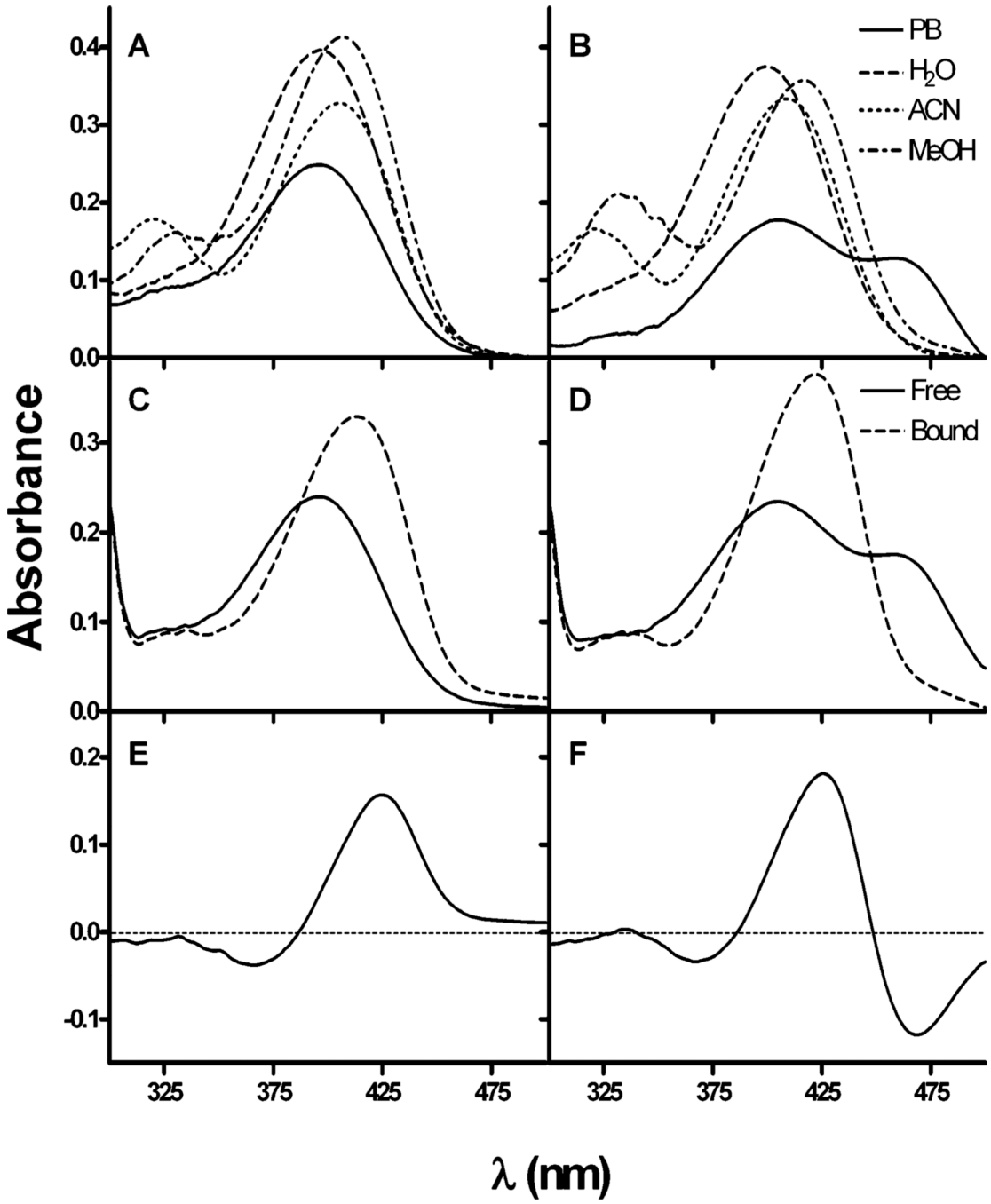

Figure 5.

Absorption spectra of DMXBA **18** and 2-MeO and 4-OHBA **21** in the presence of different solvents and bound to the AChBP. (A) and (B) DMXBA and 2-MeO and 4-OHBA in the presence of methanol (ε_r = 33.0), acetonitrile (ε_r = 37.5), H_2O (ε_r = 80.0), and a 0.1 M phosphate buffer (PB) at pH 7.0 (ε_r ~ 80.0). (C) and (D) DMXBA and 2-MeO and 4-OHBA absorbance of ligands in a 0.1 M phosphate buffer at pH 7.0 (−), bound to AChBP. (E) and (F) Difference spectra reflecting DMXBA (E) and 2-MeO, 4-OHBA (F) in mixed (sample cuvette) and unmixed (reference cuvette) tandem compartments. Substituted BAs (20 μM) were used in the presence of 1.2 M excess of AChBP sites in 0.42 path length cuvettes. The difference spectra were measured comparing mixed and unmixed 20 μM BA and 24 μM

AChBP in the same tandem cuvettes. The absorption values in the difference spectra are corrected for a 1 cm path length.

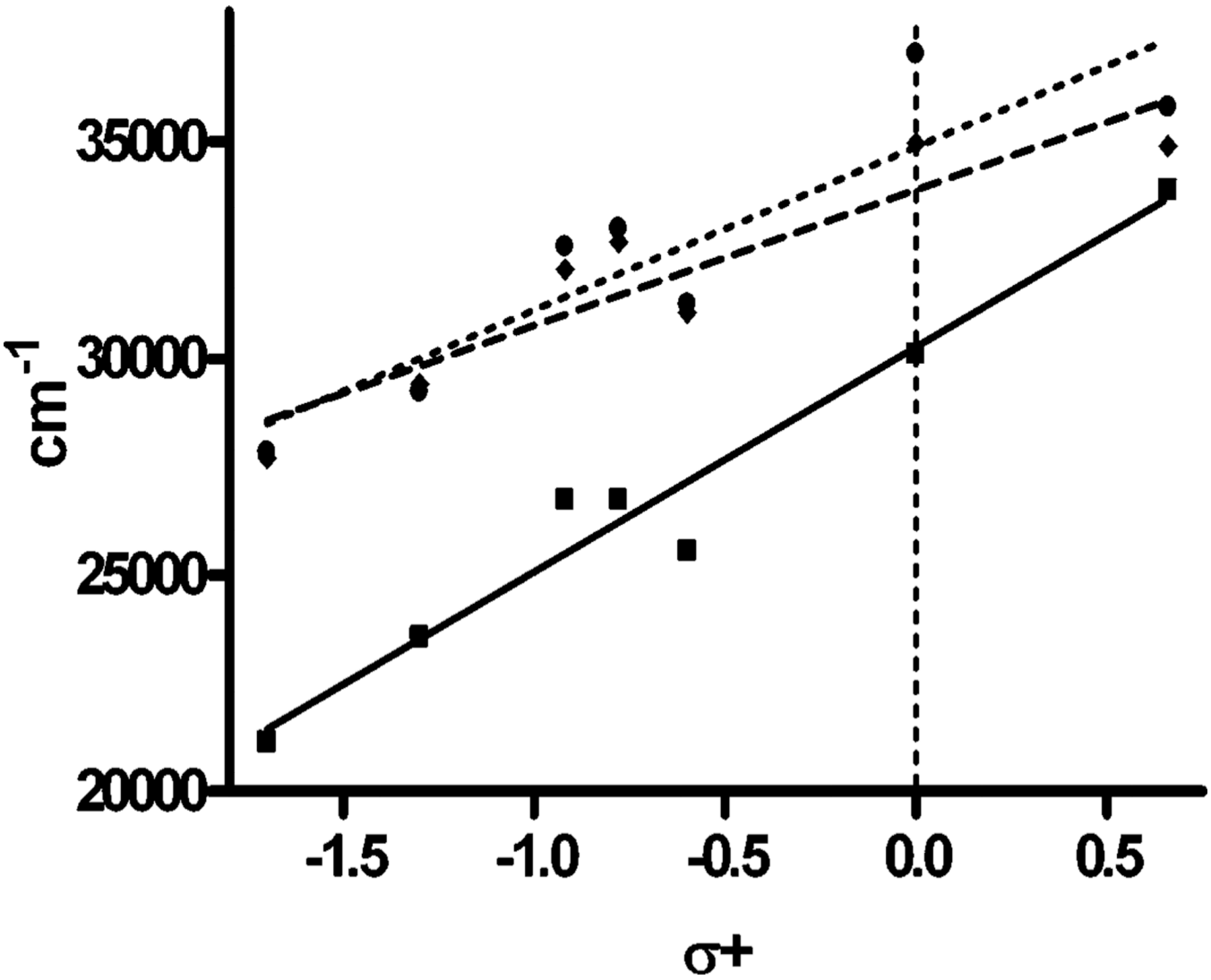

Figure 6.

Relationship between the absorption maximum of the substituted anabaseines and the Hammett substituent parameter (σ^+) (22) in the presence of various solvents ($r^2 > 0.8$). Values of σ^+ used: 0.0 for BA **7**, −1.7 for 4-DMABA **16**, −1.3 for 4-NH_2BA **15**, −0.92 for 4-OHBA **12**, −0.78 for 4-MeOBA **13**, −0.6 for 4-MeSBA **14**, and 0.66 for 4-CNBA **17**. Solvents: 0.1 M pH 7.0 phosphate buffer (■, solid line), DMSO (♦, dashed line), DMF (●, dotted line). The dashed vertical line shows the position of the unsubstituted BA.

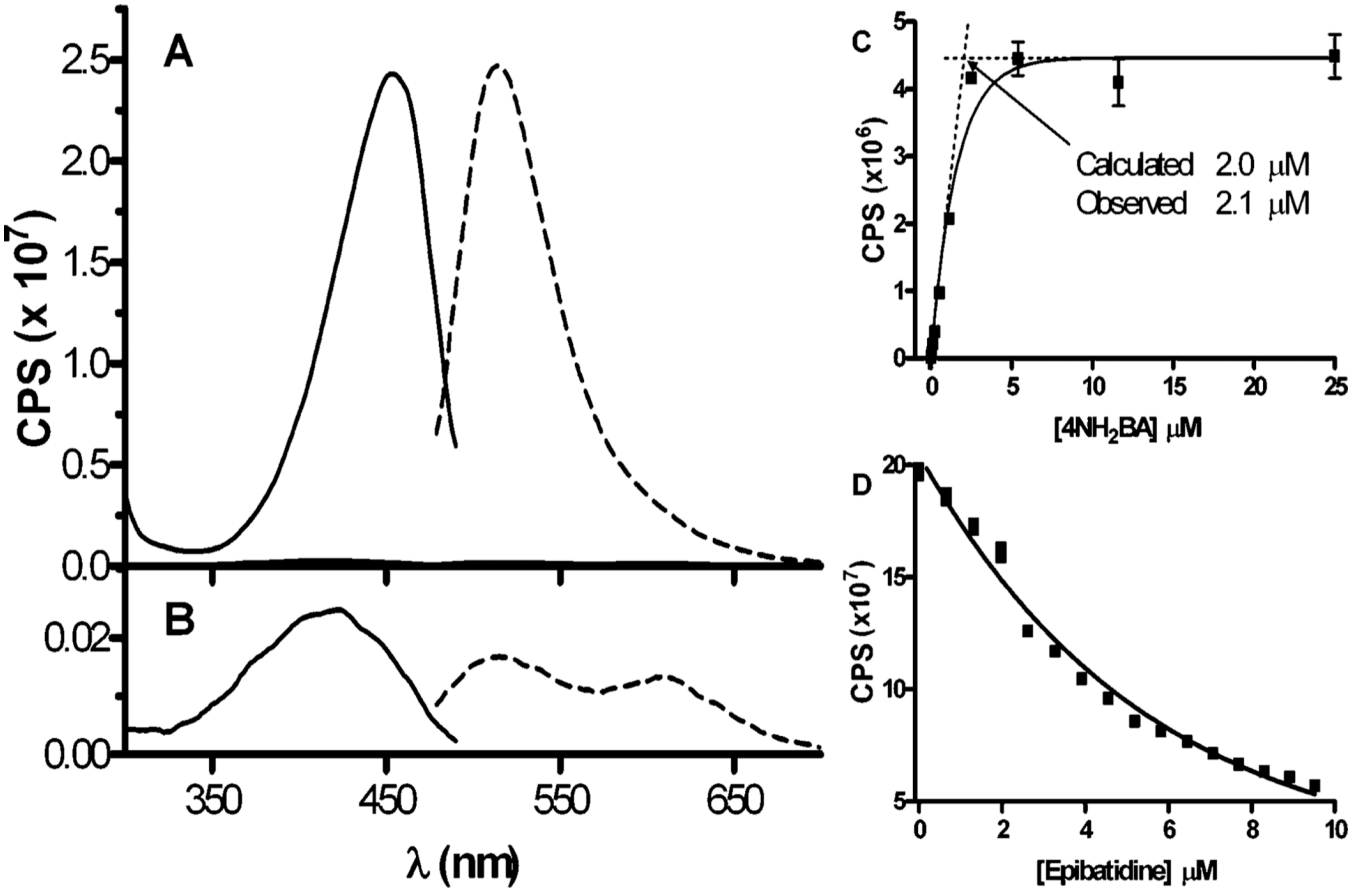

Figure 7.

Fluorescence properties of the free and *Ls* bound anabaseine derivative 4-NH_2BA **15** in a 0.1 M phosphate buffer at pH 7.0. (A) Excitation (—) and emission (---) spectra of 10 μM 4-NH_2BA bound to *Ls*-AChBP shows prominent peaks; (B) expansion of the fluorescence of the free species, also at 10 μM concentration. (C) Titration of 2 μM (binding sites) *Ls*-AChBP with varying concentrations of 4-NH_2BA (λ_{ex} = 420 nm, λ_{em} = 520 nm). Because the AChBP concentration greatly exceeds the K_d value (0.77 nM), the titration gives an estimate of the stoichiometry of binding. (D) Dissociation of 4-NH_2BA from *Ls*-AChBP with increasing concentrations of epibatidine demonstrating the complete loss of fluorescence by the competing ligand (λ_{ex} = 420 nm, λ_{em} = 520 nm).

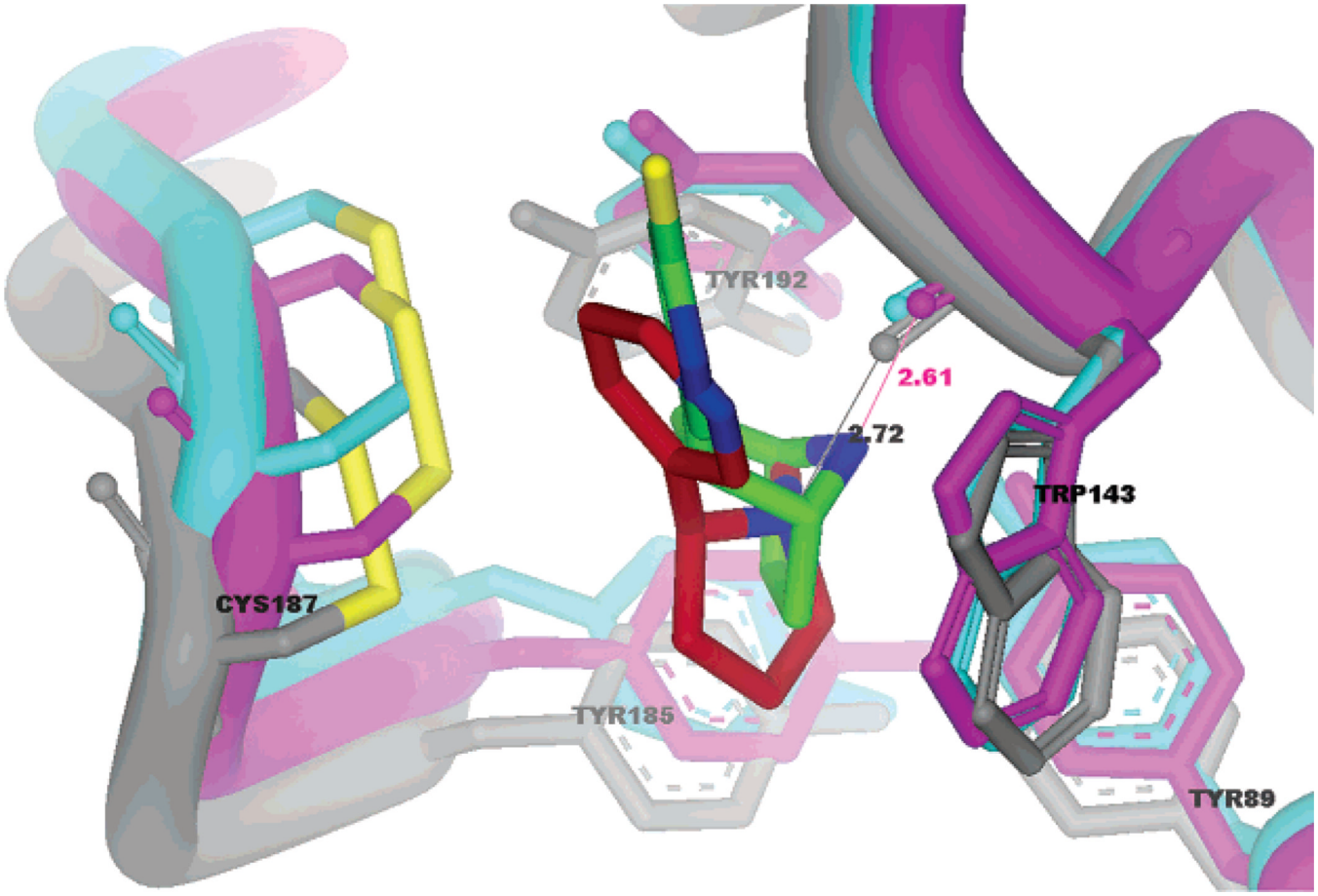

Figure 8.

Structural alignment of the crystallographic coordinates for *Ls*-AChBP (gray) with nicotine (red) bound (pdb ID 1UW6 (5)), *Ac*-AChBP (magenta) with epibatidine (green) bound (pdb ID 2BYQ (6)), and *Bt*-AChBP (cyan) with CHAPS (not shown) in the binding site (pdb ID 2BJ0 (3)). The bound ligand is enveloped by the side chains of Trp 143 and Tyr 192 using *Ls* numbering with other proximal aromatic side chains. Bond distances between the carbonyl oxygen of Trp 143 and the protonatable nitrogen of nicotine and epibatidine are shown.

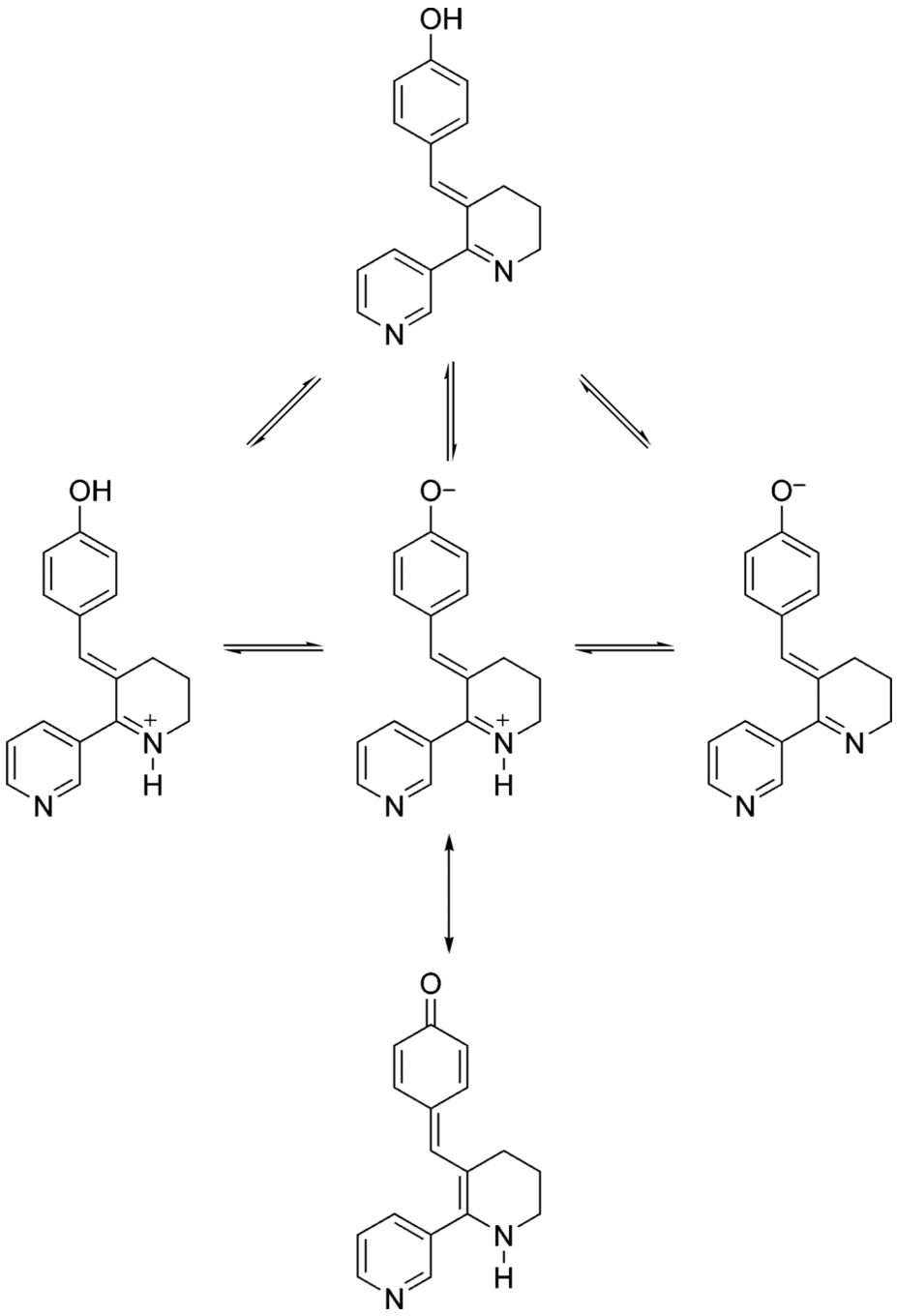

Scheme 1. Ionization Scheme for Hydroxyl Benzylidene Anabaseinesa

[a] The equilibrium arrows denote proton addition and removal.

Table 1

Abbreviated Names of Anabaseine and Its Analogues with Their Corresponding Dissociation Constants for the Three Acetylcholine Binding Proteins from *Lymnaea stagnalis* (*Ls*), *Aplysia californica* (*Ac*), and *Bulinus truncatus* (*Bt*)

						Lymnaea stagnalis		*Aplysia californica*		*Bulinus truncatus*	
comd	**abbreviation**	**R_1**	**R_2**	**R_3**	**R_4**	**K_d (nM) ± S.E.M.**	**n_d**	**K_d (nM) ± S.E.M.**	**n_H**	**K_d (nM) ± S.E.M.**	**n_H**
1	nicotine					100 ± 5	1.03	260 ± 15	1.11	72 ± 3	0.93
2	epibatidine					0.30 ± 0.05	0.99	6.8 ± 2	1.01	0.65 ± 0.09	0.99
3	anabaseine					240 ± 21	1.03	> 1000		830 ± 64	1.09
4	PTHP[a]					220 ± 5	0.91	> 1000		> 1000	
5	DMXBzAi[b]					150 ± 12	0.92	130 ± 16	1.13	250 ± 40	1.05
6	DMXB IsoA[c]					110 ± 27	1.10	890 ± 43	1.17	> 1000	
7	BA	-H	-H	-H	-H	14 ± 1	1.01	9 ± 2.1	1.00	120 ± 88	1.11
8	2-OHBA[d]	-OH	-H	-H	-H	21 ± 4	1.11	95 ± 6	1.03	290 ± 140	0.96
9	2-MeOBA	$-OCH_3$	-H	-H	-H	7 ± 0.4	0.83	88 ± 8	0.89	35 ± 7	0.90
10	3-OHBA	-H	-OH	-H	-H	13 ± 2	0.89	14 ± 0.9	1.31	73 ± 7	1.30
11	3-MeOBA	-H	$-OCH_3$	-H	-H	21 ± 4	1.10	31 ± 2	1.12	280 ± 110	1.07
12	4-OHBA	-H	-H	-OH	-H	0.57 ± 0.13	0.94	5 ± 0.8	0.95	36 ± 7	0.97
13	4-MeOBA	-H	-H	$-OCH_3$	-H	20 ± 2	1.07	95 ± 10	1.07	270 ± 15	1.05
14	4-MeSBA	-H	-H	$-SCH_3$	-H	19 ± 1	1.03	140 ± 6	1.05	350 ± 120	0.97
15	4-NH_2BA	-H	-H	$-NH_2$	-H	0.77 ± 0.07	0.92	3 ± 0.57	0.99	33 ± 8	1.05
16	4-DMABA	-H	-H	$-N(CH_3)_2$	-H	4 ± 0.14	0.91	26 ± 3	0.99	73 ± 1	0.93
17	4-CNBA	-H	-H	-CN	-H	120 ± 3	1.04	> 1000		> 1000	
18	DMXBA	$-OCH_3$	-H	$-OCH_3$	-H	19 ± 1	1.15	330 ± 58	1.03	59 ± 8	1.22
19	2-OH, 4-MeOBA	-OH	-H	$-OCH_3$	-H	12 ± 3	0.87	220 ± 26	0.98	90 ± 9	1.08
20	2-F, 4-MeOBA	-F	-H	$-OCH_3$	-H	12 ± 0.01	1.19	250 ± 2	1.14	290 ± 5	1.19
21	2-MeO, 4-OHBA	$-OCH_3$	-H	-OH	-H	0.43 ± 0.03	0.84	3 ± 0.96	0.76	22 ± 4	0.97
22	2, 4-DiOHBA	-OH	-H	-OH	-H	0.77 ± 0.32	1.03	6 ± 0.15	0.98	93 ± 36	0.93
23	3, 4-DiOEBA	-H		$-OCH_2O-$	-H	20 ± 3	1.08	47 ± 5	0.84	130 ± 25	0.85
24	4-DMANA		$-C_4H_4-$	$-N(CH_3)_2$	-H	51 ± 3	1.16	510 ± 220	1.20	170 ± 10	1.33

Biochemistry. Author manuscript; available in PMC 2011 November 22.

						Lymnaea stagnalis		*Aplysia californica*		*Bulinus truncatus*	
comd	**abbreviation**	**R_1**	**R_2**	**R_3**	**R_4**	**K_d (nM) ± S.E.M.**	**n_d**	**K_d (nM) ± S.E.M.**	**n_H**	**K_d (nM) ± S.E.M.**	**n_H**
25	TMXBA	-OCH_3	-H	-OCH_3	-OCH_3	140 ± 10	0.90	> 1000		550 ± 5	0.98
26	2, 6-DiMeO, 4-OHBA	-OCH_3	-H	-OH	-OCH_3	34 ± 2	0.93	420 ± 30	1.00	450 ± 0	1.01

[a]2-(3-Pyridyl)-3,4,5,6-tetrahydropyrimidine.

[b]3-(2,4-Dimethoxybenzyl)-(±) anabaseine.

[c]2-(4-Pyridyl)-3-(2,4-dimethoxybenzylidene)-4,5,6,-tetrahydropyridine.

[c]All substitution numbers (compounds **8**–**26**) refer to positions on the 3-benzylidene ring.

Biochemistry. Author manuscript; available in PMC 2011 November 22.

Table 2

pK_a Values and Wavelength Maxima at pH 5.0 and 9.0 for Representative Benzylidene Anabaseines[a]

compd no.	abbreviation	pK_a	λ_{max} at pH 5.0	λ_{max} at pH 9.0	$\Delta\ \lambda_{max}$
7	BA	7.37	330	279	−51
12	4-OHBA	7.09	372	448	76
15	4-NH_2BA	8.11	420	322	−98
16	4-DMABA	8.20	471	344	−127
18	DMXBA	7.61	395	317	−78
19	2-OH, 4-MeOBA	7.04	344	471	127
21	2-MeO, 4-OHBA	7.12	396	462	66

[a]The measurements were conducted in a 0.1 M phosphate-pyrophosphate buffer.

Biochemistry. Author manuscript; available in PMC 2011 November 22.

Table 3

Wavelength Maxima for Free and *Lymnaea* (*LS*)- and *Aplysia* (*Ac*)-Bound Benzylidene Anabaseines

compd no.	abbreviation	buffer	*Ls*	$\Delta \lambda_{max}$	*Ac*	$\Delta \lambda_{max}$
7	BA	333	341	8	335	2
12	4-OHBA	374	400	25	436	62
15	4-NH_2BA	426	454	28	435	9
16	4-DMABA	474	479	5	476	2
18	DMXBA	397	413	16	408	11
19	2-OH, 4-MeOBA	398	420	22	411	15
21	2-MeO, 4-OHBA	406	417	11	417	11